rpS6 Regulates Blood-Testis Barrier Dynamics Through Arp3-Mediated Actin Microfilament Organization in Rat Sertoli Cells. An In Vitro Study

Ka-Wai Mok, Haiqi Chen, Will M. Lee, and C. Yan Cheng

The Mary M. Wohlford Laboratory for Male Contraceptive Research (K.-W.M., H.C., C.Y.C.), Center for Biomedical Research, Population Council, New York, New York 10065; and School of Biological Sciences (W.M.L.), University of Hong Kong, Hong Kong, China

In the seminiferous epithelium of rat testes, preleptotene spermatocytes residing in the basal compartment are transported across the blood-testis barrier (BTB) to enter the adluminal compartment at stage VIII of the epithelial cycle. This process involves redistribution of tight junction (TJ) proteins via reorganization of actin cytoskeleton in Sertoli cells that serves as attachment site for adhesion protein complexes. Ribosomal protein S6 (rpS6), a downstream molecule of mTORC1 (mammalian target of rapamycin complex 1), participates in this process via a yet-to-be defined mechanism. Here, we constructed an rpS6 quadruple phosphomimetic mutant by converting Ser residues at 235, 236, 240, and 244 to Glu via site-directed mutagenesis, making this mutant constitutively active. When this rpS6 mutant was overexpressed in Sertoli cells cultured in vitro with an established TJ barrier mimicking the BTB in vivo, it perturbed the TJ permeability by downregulating and redistributing TJ proteins at the cell-cell interface. These changes are mediated by a reorganization of actin microfilaments, which was triggered by a redistribution of activated actin-related protein 3 (Arp3) as well as changes in Arp3-neuronal Wiskott-Aldrich Syndrome protein (N-WASP) interaction. This in turn induced reorganization of actin microfilaments, converting them from a "bundled" to an "unbundled/branched" configuration, concomitant with a reduced actin bundling activity, thereby destabilizing the TJ-barrier function. These changes were mediated by Akt (transforming oncogene of v-akt), because an Akt knockdown by RNA interference was able to mimic the phenotypes of rpS6 mutant overexpression at the Sertoli cell BTB. In summary, this study illustrates a mechanism by which mTORC1 signal complex regulates BTB function through rpS6 downstream by modulating actin organization via the Arp2/3 complex, which may be applicable to other tissue barriers. **(*Endocrinology* 156: 1900–1913, 2015)**

Spermatogenesis is a complex and tightly regulated cellular process that takes places in the epithelium of seminiferous tubules in mammalian testes (1–3). Because the seminiferous epithelium is anatomically divided by the blood-testis barrier (BTB) into the basal and the adluminal compartments, one of the crucial cellular events during spermatogenesis is to allow the transport of preleptotene spermatocytes across the immunological barrier at stage VIII of the epithelial cycle, such as in the rat testis (4–6). Studies by morphological analysis (7–9) and by biochemical assays of endocytosis, transcytosis, and recycling coupled with electron microscopy (9, 10) have shown that the

ISSN Print 0013-7227 ISSN Online 1945-7170
Printed in U.S.A.

Received September 25, 2014. Accepted February 19, 2015.
First Published Online February 25, 2015

Abbreviations: Akt, transforming oncogene of v-akt encoding an Ser/Thr protein kinase also known as protein kinase B (PKB); Arp2/3 complex; actin-related protein 2/3 complex; BTB, blood-testis barrier; Co-IP, coimmunoprecipitation; c-Src, cellular Rous sarcoma virus transforming oncogene encoding a non-receptor protein tyrosine kinase; c-Yes, cellular Yamaguchi sarcoma viral oncogene homolog 1 encoding a non-receptor protein tyrosine kinase; Cy3, Cyanine 3; DAPI, 4′,6-diamidino-2-phenylindole; Eps8, epidermal growth factor receptor pathway substrate 8; ES, ectoplasmic specialization; FAK, focal adhesion kinase; IF, immunoprecipitation; IHC, immunohistochemistry; mTORC1, mammalian target of rapamycin complex 1; mTORC2, mammalian target of rapamycin complex 2; N-WASP, neuronal Wiskott-Aldrich Syndrome protein; p, phosphorylated (activated); rpS6, ribosomal protein S6; RNAi, RNA interference; siRNA, small interfering RNA; TJ, tight junction; WT, wild-type; ZO-1, zonula occludens-1.

assembly of a "new" BTB underneath the preleptotene spermatocytes connected in clones via intercellular bridges being transported across the immunological barrier is complete before the "old" BTB that lies above the preleptotene spermatocytes is disassembled. This, thus, provides a novel mechanism for the transport of preleptotene spermatocytes across the BTB at stage VIII of the cycle without compromising the integrity of the immunological barrier. This concept has been further confirmed by the use of confocal microscopy using pertinent markers of tight junction (TJ) integral membrane proteins such as claudin-3 and claudin-11 (11). However, the precise molecular mechanism that elicits the timely assembly of the new vs the disassembly of the old BTB during the transport of preleptotene spermatocytes across the immunological barrier remains unknown. Studies using biochemical assays to track endocytic vesicle-mediated protein trafficking have shown that both cytokines (eg, TGF-β and TNFα, known to promote Sertoli cell TJ-barrier disruption) (12) and androgen (eg, testosterone, known to promote TJ-barrier integrity) (12, 13) accelerate the kinetics of protein endocytosis (10). However, cytokines promote endocytosed proteins (eg, occludin and N-cadherin) to enter the endosome-mediated protein degradation pathway, whereas testosterone directs the endocytosed BTB proteins to the transcytosis/recycling pathway (10, 14), involving c-Src (cellular Rous sarcoma virus transforming oncogene) and c-Yes (Yamaguchi sarcoma viral oncogene homolog 1) (15). Thus, the antagonistic effects of cytokines/c-Src vs testosterone/c-Yes provide a novel mechanism, by which these biomolecules can effectively remodel BTB to facilitate spermatocyte transport at the BTB.

Mammalian target of rapamycin complex 1 (mTORC1) and mTORC2 are 2 signaling complexes that possess antagonistic effects on BTB function in which mTORC1 perturbs (16), whereas mTORC2 promotes (17) Sertoli cell TJ-permeability barrier, illustrating that these 2 signaling complexes modulate the tightly coordinated events of BTB disassembly and assembly during the transport of preleptotene spermatocytes at the immunological barrier. This concept is indeed supported by the spatiotemporal expression of the key downstream signaling molecule or component protein of the mTORC1 and mTORC2, namely p-rpS6 (phosphorylated-rpS6) and rictor, respectively, at the BTB in the rat testis (16, 17). However, the mechanism by which mTORC1 disrupts BTB function via rpS6 remains unknown. It is noted that TJ and basal ectoplasmic specialization (ES) (a testis-specific adherens junction), which constitute the BTB, are both F-actin-rich ultrastructures, and they are typified by the presence of an array of actin microfilaments sandwiched between the apposing Sertoli cell plasma membranes and the cisternae of endoplasmic reticulum (12, 18); and mTOR signaling complexes (ie, mTORC1 and mTORC2) have recently been shown to be involved in the organization of actin microfilaments (19, 20). We, thus, sought to examine whether rpS6, in particular its phosphorylated/activated form p-rpS6, under the regulation of mTORC1 that exerts its BTB disruptive effect is mediated through actin-based cytoskeleton. Here, a constitutively active quadruple phosphomimetic mutant of p-rpS6 was prepared to assess its effects on F-actin organization at the Sertoli cell BTB after transfection vs the use of wild-type (WT) rpS6 and control (empty mammalian expression vector). We also examined whether the recently identified upstream regulator of Akt (transforming oncogene of v-akt, also known as protein kinase B) of mTORC1 (21) is also involved in these events. In short, we sought to test the hypothesis that p-rpS6 which promotes Sertoli cell TJ-barrier disruption is exerting its effects on the organization of actin microfilaments, mediated by the intricate action of branched actin polymerization-inducing protein Actin-related protein 2/3 (Arp2/3)/Neuronal Wiskott-Aldrich Syndrome protein (N-WASP) complex. These findings would help us to better understand the regulation of BTB remodeling during the epithelial cycle of spermatogenesis.

Materials and Methods

Animals and antibodies

The use of Sprague-Dawley rats (Charles River Laboratories) for experiments reported here was approved by the Rockefeller University Institutional Animal Care and Use Committee with protocol numbers 09016 and 12506. Rats were euthanized by CO_2 asphyxiation using slow (20%–30% per min) displacement of chamber air with compressed carbon dioxide in a euthanasia chamber (Braintree Scientific). Antibodies were obtained commercially unless otherwise specified and listed in Supplemental Table 1.

Construction of WT and rpS6 quadruple constitutively active phosphomimetic mutant (active rpS6) in mammalian expression vector

To clone the WT rpS6 cDNA, the full-length coding sequence of WT rat rpS6 (GenBank accession number, NM_017160.1) was amplified from rat Sertoli cell cDNA by PCR using primers listed in Table 1. The rpS6 full-length cDNA was cloned into the *Mlu*I/*Xba*I site of the mammalian expression vector pCI-neo (Promega). This full-length cDNA clone was confirmed by direct nucleotide sequence analysis at Genewiz. The rpS6 quadruple constitutively active phosphomimetic mutant was obtained by site-directed mutagenesis using an approach as detailed elsewhere (22), in which Ser residues at 235, 236, 240, and 244 of rpS6 were substituted by Glu by using primer pairs containing the mutation sites (Table 1) and the WT construct as the template. rpS6 mutation were then cloned into the pCI-neo vector at

Table 1. Primers Used to Obtain the rpS6 WT Clone or Quadruple Phosphomimetic Mutant

Target Gene	GenBank Accession Number	Primer Sequence (5′-3′)	Nucleotide Position	Size in b.p.
Primers				
rpS6	NM_017160.1	S, 5′-AA*ACGCGT*ATGAAGCTGAATATCTCCTTC-3′	1–21	766
		AS, 5′-AA***TCTAGA***TTATTTTTGACTGGACTCAGA-3′	730–750	
Mutagenic primers				
rpS6	NM_017160.1	S, 5′-AA*ACGCGT*ATGAAGCTGAATATCTCCTTC-3′	1–21	766
		AS, 5′-AA***TCTAGA***TTATTTTTGACTGGACTCTTCTTTAGAAGTTTCAGCTCTCAGTTCTTC-3′	703–750	

Underlined italicized sequences and underlined boldface/italicized sequences indicate *Mlu*I and *Xba*I restriction enzyme recognition site, respectively, which were added for cloning of the WT rpS6 or constitutively active quadruple phosphomimetic rpS6 mutant into the pCI-neo mammalian expression vector. Underlined sequences indicate mutation sites in which Ser residues were replaced by Glu to obtain the quadruple phosphomimetic rpS6 mutant. S, sense; AS, antisense.

the *Mlu*I/*Xba*I. Mutation sites in this quadruple phosphomimetic mutant was verified by direct DNA sequencing at Genewiz. Plasmid DNA was then prepared with a HiSpeed Plasmid Midi kit (QIAGEN). To confirm successful transfection in overexpression experiments, plasmid DNA was labeled with Cyanine 3 (Cy3) using a Label*IT* Tracker Intracellular Nucleic Acid Localization kit (Mirus).

Isolation of Sertoli cells for primary cultures for overexpression of rpS6 WT, quadruple constitutively active phosphomimetic mutant vs control (empty) vector, and for knockdown of Akt1/2 by RNA interference (RNAi)

Sertoli cells were isolated from testes of 20-day-old rats as described (23). Sertoli cells were plated on Matrigel (diluted 1:7 in medium; BD Biosciences)-coated culture plates, coverslips and Millicell HA 12-mm culture inserts (Millipore) at a density 0.5, 0.05, and 1×10^6 cells/cm^2, respectively. Sertoli cells were cultured in serum-free F12/DMEM (Ham's F12 Nutrient Mixture/DMEM) (Sigma-Aldrich) supplemented with growth factors, bacitracin, and gentamicin as described (23) in a humidified atmosphere of 95% air/5% CO_2 (vol/vol) at 35°C. On day 2 after a functional TJ-permeability barrier was established, transfection of different plasmid DNA (~0.45-μg DNA per 10^6 Sertoli cells) was performed for 18 hours using Effectene Transfection reagent (QIAGEN) as the transfection medium according to the manufacturer's instructions. For the knockdown of Akt1 and Akt2, Akt1- and Akt2-specific small interfering RNA (siRNA) duplexes vs nontargeting control siRNA duplexes were used to transfect Sertoli cells on day 3 using RiboJuice siRNA transfection reagent (Novagen, EMD Bioscience) for 24 hours according to the manufacturer's instructions as described (17). siRNA duplexes at 100nM were used for transfection experiments intended for lysate preparation and fluorescence microscopy, whereas 200nM was used for cells for assessing the TJ-permeability barrier function. These concentrations of siRNA duplexes were selected based on results of pilot experiments because a distinctive phenotype was detected. The sequence of siRNA duplex that specifically targeted Akt1 was 5′-CCAGGUAUUUUGAUGAGGAtt-3′ (s127430; Ambion) and that for Akt2 was 5′-GGUAUAAAGAGAGACCUGAtt-3′ (s129224; Ambion). Nontargeting siRNA duplex (Silencer Select Negative Control 1 siRNA; Ambion) served as the negative control. Cells were harvested 2 days after transfection of Sertoli cells with either plasmid DNA or siRNA duplexes for fluorescence microscopy or preparation of lysates. Transepithelial electrical resistance that quantified the TJ-permeability barrier across the Sertoli cell epithelium in bicameral units was recorded daily throughout the period of culture as described (24). Sertoli cells cultured in vitro under the conditions described above were shown to establish a functional TJ-permeability barrier with ultrastructures of TJ, basal ES, gap junction, and desmosome (25–27), mimicking the Sertoli cell BTB in vivo. This in vitro system has been widely used by investigators in the field to study Sertoli cell BTB function (28–33), and findings based on this in vitro system have been confirmed in studies in vivo (32, 34–37), illustrating that findings based on this system is physiologically relevant to the testis in vivo.

Lysate preparation and immunoblotting

Lysate was prepared from Sertoli cells using immunoprecipitation (IP) lysis buffer (50mM Tris [pH 7.4], at 22°C, containing 0.15M NaCl, 1% Nonidet P-40 [vol/vol], 1mM EGTA, 2mM N-ethylmaleimide, and 10% glycerol [vol/vol]) supplemented with protease inhibitor mixture (Sigma-Aldrich) and phosphatase inhibitor mixture II and III (Sigma-Aldrich) at a dilution of 1:66.7 as specified by the manufacturer. Protein concentration was estimated using a Bio-Rad D_c Protein Assay kit using BSA as a standard. Approximately 35 μg of protein from lysate were used per lane for immunoblotting (16). Immunoblot analysis was performed using a chemiluminescence kit prepared in-house, and images were acquired with a Fujifilm LAS4000 mini Luminescent Image Analyzer (38).

Coimmunoprecipitation (Co-IP)

Co-IP used to assess changes in protein-protein interaction after overexpression of quadruple rpS6 phosphomimetic mutant vs WT rpS6 and control (empty) vector, or the knockdown of Akt was performed as described (17, 22). In brief, to assess changes in the association between 1) N-WASP and Arp3 as well as 2) α-catenin and actin, after transfection of plasmid DNA or siRNA duplexes in Sertoli cells, 400-μg protein of cell lysate obtained 2 days after transfection was incubated with 1.5-μg normal rabbit IgG for 2 hours, to be followed by 2 hours of incubation with 15-μL Protein A/G Plus (Santa Cruz Biotechnology, Inc) in a preclearing step to eliminate nonspecific protein-IgG interaction. Thereafter, supernatant was obtained by centrifugation (1000*g*, 5 min) and was then incubated with the IP antibody (Supplemental Table 1) overnight at room temperature in a rotating rocker for immunoprecipitation. IP antibody was substituted

with normal rabbit IgG for negative control. Thereafter, lysate was incubated with 20-μL Protein-A/G Plus for 6 hours to obtain the immuno-complexes, which were extracted by sodium dodecyl sulfate sample buffer for immunoblot analysis (17, 22).

Immunohistochemistry (IHC) and dual-labeled immunofluorescence analysis

For IHC, testes were fixed in Bouin's fixative (Polysciences), embedded in paraffin, and sectioned to 5 μm; after antigen retrieval, color development was performed using 3,3-diaminobenzidine as described (24). Dual-labeled immunofluorescence analysis was performed using frozen sections of testes (7-μm thickness) and corresponding primary antibodies (Supplemental Table 1) and Alexa Fluor-conjugated secondary antibodies (red fluorescence, Alexa Fluor 555 and green fluorescence, Alexa Fluor 488; Invitrogen) (16, 21). To visualize F-actin, sections or cells were incubated with Cy3 or fluorescein isothiocyanate-conjugated phalloidin (Sigma-Aldrich) at 1:50 dilution together with corresponding secondary antibodies. Fluorescence images were obtained using a Nikon Eclipse 90i Fluorescence Microscope equipped with a Nikon DS-Qi1Mc digital camera, using Nikon NIS Elements Imaging Software (version 3.2) (Nikon Instruments, Inc). Image overlay to assess protein colocalization was performed using PhotoShop in Adobe Creative Suite (version 3.0) software package. All sections of testes or Sertoli cells within an experimental group were processed simultaneously in a single experimental session to eliminate interexperimental variations.

Actin bundling assay

Lysates of transfected Sertoli cells were obtained using Tris lysis buffer (20mM Tris [pH 7.5] at 22°C, containing 20mM NaCl and 0.5% [vol/vol] Triton X-100, freshly supplemented with Protease Inhibitor Mixture [Sigma-Aldrich] and Phosphatase Inhibitor Mixtures 2 and 3 [Sigma-Aldrich], freshly added to the lysis buffer using an inhibitor cocktail to buffer ratio of 1:66.7) by passing through cells resuspended in Tris lysis buffer in syringes with 29-gauge needles for 20 times. Cleared supernatant was obtained by centrifugation at 20 817*g* for 2.5 hours at 4°C, and all samples were diluted to the same protein concentration to 5 μg/μL using the Tris lysis buffer. F-actin was prepared as follows. Pyrene-labeled muscle actin (cytoskeleton) at 10 mg/mL was first diluted to 1 mg/mL with general actin buffer (5mM Tris·HCl [pH 8.0] containing 0.2mM $CaCl_2$ and freshly supplemented with 0.2mM ATP). Diluted actin was then incubated on ice for 30 minutes to obtain G-actin. This was followed by the addition of 0.1 vol of 10× actin polymerization buffer (100mM Tris·HCl [pH 7.5] containing 500mM KCl, 20mM $MgCl_2$, and 10mM ATP) to initiate actin polymerization. Mixture was incubated at room temperature for 1 hour to yield an F-actin stock of approximately 21μM. Cell lysate was added to the F-actin stock prepared above in a 1:4 ratio (lysate to F-actin) to a final reaction volume of approximately 50 μL in each sample tube and was incubated at room temperature for 30 minutes to assess its activity to bundle actin filaments. This was followed by centrifugation at 14 000*g* for 5 minutes at 24°C to pellet bundled F-actin. Supernatants containing unbundled F-actin were collected and subjected to immunoblot analysis together with the pellets that contained bundled microfilaments. All samples within a single experiment were processes simultaneously to eliminate interexperimental variations.

Actin polymerization assay

Assay polymerization assay to assess the kinetics of actin polymerization was performed as described (22). In brief, lysates of Sertoli cells were diluted to the same protein concentration between samples. The effect of these lysates on actin polymerization was immediately assayed using an Actin Polymerization Biochem kit (cytoskeleton). Reactions consisted of 1) pyrene-labeled muscle actin in general actin buffer, 2) Sertoli cell lysate prepared using the Tris lysis buffer, and 3) actin polymerization buffer, and reaction was performed according to the manufacturer's protocol. Polymerization of pyrene-labeled actin was estimated by an increase in fluorescence emission at 395–440 nm, which was measured in a black-bottomed 96-well plate (via top reading) in a Molecular Devices FilterMax F5 Multi-Mode Microplate Reader. A kinetic reading was taken at room temperature every 20 seconds for approximately 280 cycles using the Multi-Mode Analysis Software package from Molecular Devices. The rate of increase in fluorescence intensity during the initial linear phase of the reaction (first 14 min) was estimated by linear regression analysis using Microsoft Excel.

Statistical analysis

Statistical analysis was performed using GB-STAT software package (version 7.0; Dynamic Microsystems) using two-way ANOVA followed by Newman-Keul's test.

Results

Stage-specific expression of p-rpS6 S235/236 and p-rpS6 S240/S244 at the BTB

The activated p-rpS6 S235/S236 was localized near the basement membrane when examined by IHC, consistent with its localization at the BTB with its expression mostly limited to stage VIII–IX of the epithelial cycle (Figure 1A). This finding is consistent with an earlier study reporting the localization of p-rpS6 in the rat testis (16). Here, we also demonstrated that p-rpS6 S240/S244 displayed similar pattern of stage-specific localization at the BTB, also highly expressed at stage VIII–IX (Figure 1A), coinciding with BTB remodeling at these stages to facilitate the transport of preleptotene spermatocytes across the immunological barrier. These findings, thus, support the postulate that an up-regulation of p-rpS6 correlates with the events of BTB restructuring. Interestingly, both p-rpS6 S235/S236 and p-rpS6 S240/S244 also highly expressed at the apical ES at the Sertoli-spermatid interface, most prominently at stage VII but considerably diminished at stage VIII and virtually undetectable at other stages of the cycle (Figure 1A). Using specific markers of the BTB, including zonula occludens-1 (ZO-1, a TJ adaptor protein) and Epidermal growth factor receptor pathway substrate 8 (Eps8, an actin barbed end capping and mi-

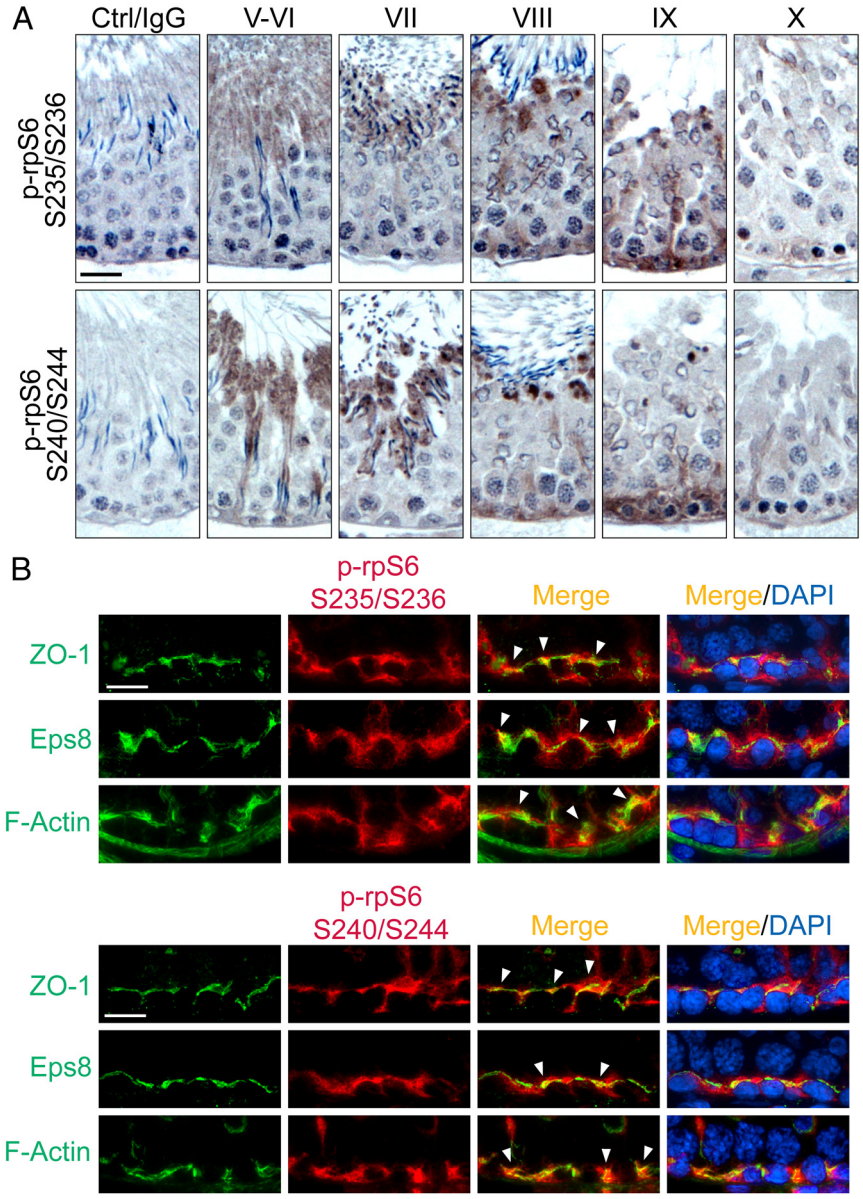

Figure 1. Immunohistochemical localization of p-rpS6-S235/S236 and p-rpS6-S240/S244 in adult rat testes. A, Using paraffin sections, localization of p-rpS6-Ser235/Ser236 (red fluorescence) vs p-rpS6-Ser240/Ser244 (red fluorescence) in the seminiferous epithelium was examined, in which p-rpS6 appeared as brownish precipitates near the basement membrane, consistent with their localization at the BTB. Phosphorylation of rpS6 at these 4 sites appeared at stage VIII and became more robust at stage IX but considerably diminished by stage X. Scale bar, 50 μm. Control (Ctrl) shown in first column is the cross-section of a testis in which the primary antibody was substituted by normal rabbit IgG, illustrating the staining specificity shown in other micrographs herein. B, Frozen sections were used to confirm their colocalization with BTB proteins ZO-1 (green fluorescence) and Eps8 (green fluorescence), and also F-actin (green fluorescence), by dual-labeled immunofluorescence analysis in which colocalized proteins (yellowish-orange to orange fluorescence) were annotated by white arrowheads. Nuclei were stained with DAPI (blue). Scale bar, 25 μm. S, Ser.

crofilament bundling protein), rpS6 S235/S236 and rpS6 S240/S244 were also found to colocalize with these proteins as well as F-actin at the BTB (Figure 1B), supporting the notion that the activated forms of rpS6 are integrated components of the BTB, associated with actin microfilaments at the site.

Overexpression of quadruple rpS6 phosphomimetic mutant perturbs Sertoli cell TJ-permeability barrier possibly mediated by Akt1/2

As shown in Figure 1, an up-regulation of p-rpS6 at the BTB at stage VIII–IX correlates with BTB restructuring at these stages, suggesting that rpS6 is a crucial regulator of BTB dynamics by inducing junction restructuring. To test this hypothesis, a quadruple phosphomimetic mutant of rpS6 was prepared by site-directed mutagenesis, in which the Ser residue in S235, S236, S240, and S244 was converted to Glu to yield a constitutively active rpS6 mutant using corresponding mutant primers (Table 1). This quadruple phosphomimetic mutant of rpS6 is referred to here as active rpS6 (pCI-neo/active rpS6). This quadruple phosphomimetic mutant was then overexpressed in Sertoli cells with an established functional TJ-permeability barrier vs control (empty) vector (pCI-neo) and wild type (WT) rpS6 (pCI-neo/rpS6, ie, WT rpS6) to assess their effects on the TJ-barrier function. It was shown that consistent with the hypothesis, overexpression of WT rpS6 indeed perturbed the Sertoli cell TJ barrier; however, overexpression of the active rpS6 was more potent in perturbing the Sertoli cell TJ-barrier function (Figure 2A). Overexpression of rpS6 or its quadruple phosphomimetic mutant in Sertoli cells was confirmed by immunoblotting using corresponding specific antibody, and it was shown that overexpression of rpS6 mutant, but not WT rpS6, induced a down-regulation of TJ proteins occludin and claudin-11, but not TJ-adaptor ZO-1 nor basal ES proteins N-cadherin and α-/β-catenin, at the BTB (Figure 2B and Supplemental Figure 1). Moreover, a down-regulation of pAkt1/2, a known upstream signaling molecule of mTORC1 (39–41), was detected, in particular in Sertoli cells overexpressed with the rpS6 quadruple phosphomimetic mutant, suggesting that Akt may be involved in this

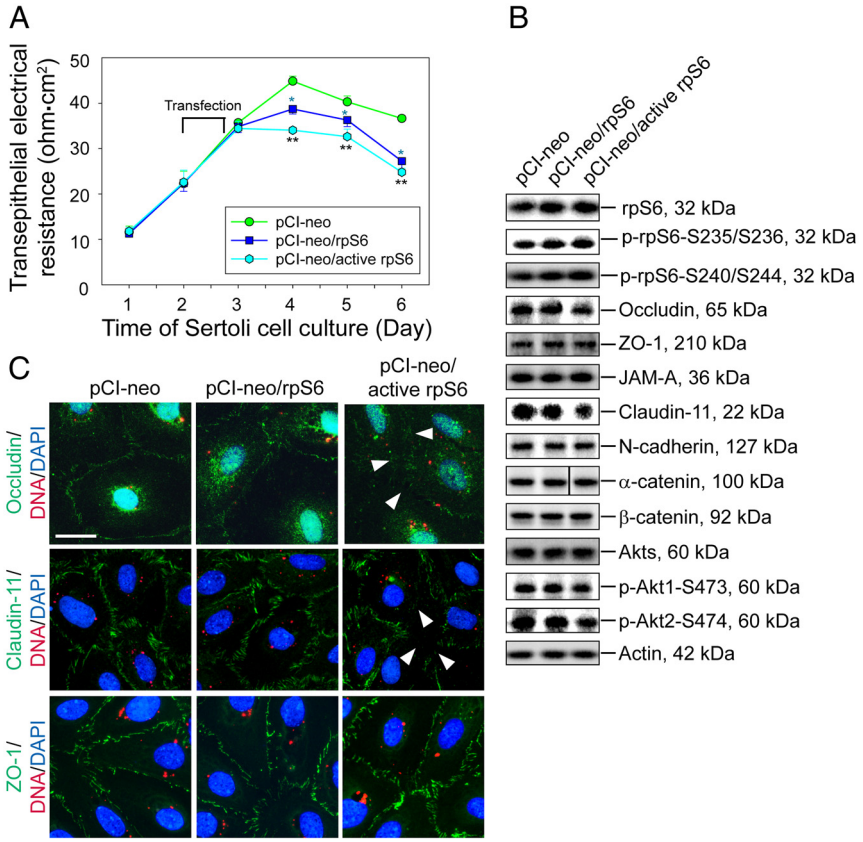

Figure 2. Overexpression of constitutively active quadruple phosphomimetic mutant of rpS6 (pCI-neo/active rpS6) vs WT rpS6 (pCI-neo/rpS6) and control (pCI-neo, empty vector) in Sertoli cells perturbs the TJ permeability in vitro via a down-regulation of p-Akt1/2. A, On day 2, Sertoli cells with a functional TJ barrier were transfected with different vectors for 18 hours. Transepithelial electrical resistance across the cell epithelium that monitored the TJ permeability was quantified daily. Each data point represents a mean ± SD of 4 replicates of a representative experiment, which was repeated 3 times using different batches of Sertoli cells with similar results. blue *, $P < .05$, WT rpS6 vs empty vector; **, $P < .01$, active rpS6 vs empty vector. B, Immunoblot analysis of different proteins. Transfection was performed on day 2, and cells were harvested on day 4 to obtain lysate for immunoblotting with β-actin served as a loading control. Data are representative findings of 4–6 experiments (see Supplemental Figure 1 for composite results). C, Changes in the localization of TJ proteins occludin (green), claudin-11 (green), and ZO-1 (green) at the Sertoli cell-cell interface were examined on day 4 after transfection of different Cy3-labeled plasmid DNA (red) on day 2 with nuclei stained with DAPI (blue). Considerably less occludin and claudin-11, but not ZO-1, were noted at the cell-cell interface after overexpression of rpS6 mutant (see white arrowheads). Scale bar, 50 μm.

event (Figure 2B and Supplemental Figure 1). Studies by dual-labeled immunofluorescence microscopy also confirmed a mislocalization of occludin and claudin-11, but not ZO-1, in Sertoli cells overexpressed with the rpS6 mutant, in which these 2 TJ integral membrane proteins no longer tightly localized to the Sertoli cell-cell interface (Figure 1C).

Overexpression of WT rpS6 or rpS6 quadruple phosphomimetic mutant perturbs the TJ barrier by shifting cortical F-actin network from bundled to branched configuration via the Arp2/3 complex

Previous study has suggested that p-rpS6 may perturb the Sertoli cell TJ-barrier function via reorganization of actin cytoskeleton at the BTB and p-rpS6 was found to structurally interacte with actin as demonstrated by Co-IP (16). p-rpS6 also colocalized with disorganized F-actin during BTB disruption, and a knockdown of rpS6 by RNAi was found to trigger F-actin reorganization in vivo and in vitro (16). To better understand how p-rpS6 regulates F-actin organization, the levels of several actin regulating proteins were investigated here. Results showed that although the steady-state levels of N-WASP (an upstream activator of the Arp2/3 complex), Arp3 (which together with Arp2 that forms the Arp2/3 complex known to induce barbed end nucleation of existing microfilaments, effective converting bundled actin filaments to a branched/unbundled configuration), Eps8, and focal adhesion kinase (FAK) remained unaltered after overexpression of WT rpS6 and its quadruple phosphomimetic mutant (Figure 3A), p-FAK-Tyr^{407}, a known regulator of Sertoli cell BTB regulator (22), was significantly up-regulated in Sertoli cells transfected with WT rpS6 or its mutant, with the mutant being more potent than the WT (Figure 3, A and B). Furthermore, when F-actin was visualized in these Sertoli cells, it was shown that overexpression of WT or rpS6 mutant led to considerably truncation of actin microfilaments in transfected Sertoli cells (Figure 3C). Besides, it was also found that WT and rpS6 mutant caused redistribution of Arp3 to the cell-cell interface (Figure 3C), where the effects of the rpS6 mutant was considerably more effective vs WT rpS6. Considering that p-FAK-Tyr^{407} was shown to promote Arp2/3 activity via N-WASP to induce F-actin branching (22, 42), we hypothesized that the induction of p-FAK-Tyr^{407} and a redistribution of Arp3 to the Sertoli cell-cell interface by WT or rpS6 mutant would shift the cortical actin filaments from bundled to branched configuration. This in turn attenuates the support of adhesion protein complexes by the bundled F-actin network, impeding the Sertoli cell TJ barrier as shown in Figure 2A. This hypothesis was supported by an increase in the association be-

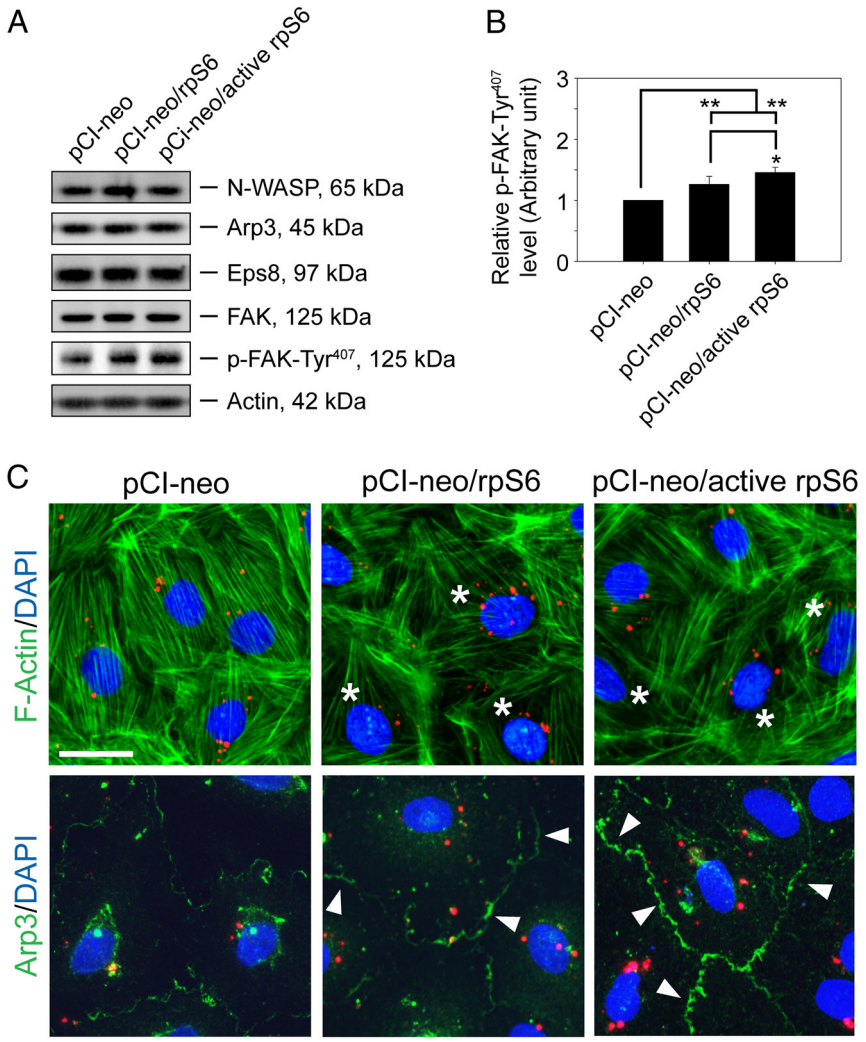

Figure 3. Overexpression of quadruple phosphomimetic mutant of rpS6 in Sertoli cell epithelium caused actin cytoskeleton reorganization by recruiting Arp3 to the cell-cell interface. Sertoli cells cultured for 2 days with an established TJ barrier were transfected with different vectors for 18 hours. Two days after transfection, cells were harvested for immunoblotting or immunofluorescence analysis (IF). A, Immunoblot analysis of proteins that are known to regulate actin dynamics with β-actin served as a loading control. Data are representative findings of 4 independent experiments. B, Histograms summarizing immunoblotting results of p-FAK-Ty^{407} as shown in A. Proteins that did not show any significant changes were not shown. Each data point was first normalized against the corresponding actin level and then against the p-FAK-Tyr^{407} in pCI-neo, which was arbitrarily set at 1. Each bar is a mean ± SD of 4 experiments. *, $P < .05$; **, $P < .01$ vs pCI-neo or pCI-neo/rpS6. C, IF was used to examine changes in F-actin (green) organization and localization of Arp3 (green) in Sertoli cells after transfection of different Cy3-labeled plasmid DNA (red) with nuclei stained with DAPI (blue). Note that after overexpression of WT rpS6 or constitutively active rpS6 mutant, the organization of F-actin was altered in which actin microfilaments were truncated and disorganized in the Sertoli cell cytosol (annotated by asterisks) vs controls. Cells transfected with either WT rpS6 or active rpS6 had more Arp3 localized at the cell-cell interface (annotated by white arrowheads), converting actin filament bundles near the cell-cell interface to a branched network, destabilizing the Sertoli cell TJ permeability, supporting data shown in Figure 2A. Scale bar, 50 μm.

tween Arp3 and its activator N-WASP in Sertoli cells after overexpression of WT or rpS6 mutant (Figure 4A), illustrating that the Arp2/3 complex was activated. Additionally, it is known that the Arp2/3 complex competes with α-catenin for binding to actin (43), thus more Arp2/3 complex that was localized to the cortical side of Sertoli cells indeed coincided with a considerable decrease in interaction between α-catenin and actin (Figure 4B). Also, this decrease in α-catenin-actin association perturbed the TJ barrier, because α-catenin is the adaptor that links adherens junction integral membrane proteins to actin-based cytoskeleton (44), such as N-cadherin at the basal ES (12). More important, the physiological consequence of such an increase in branched actin nucleation activity was assessed by an actin bundling assay, which quantified the ability of lysates from transfected Sertoli cells to bundle actin microfilaments. Bundled actin microfilaments were recovered in the pellet for analysis vs free actin microfilaments remained in the supernatant. Results showed that there was an approximately 40% and approximately 70% reduction in actin bundling activity in Sertoli cells overexpressed with WT rpS6 and rpS6 mutant vs empty vector, respectively (Figure 4C), supporting the notion that the cortical actin cytoskeleton was remodeled from "bundled" to "branched" configuration. In this context, it is of interest to note that 1) the up-regulation of p-FAK-Tyr^{407} (Figure 3, A and B), 2) the increase in the N-WASP-Arp3 association (Figure 4A), 3) the reduced α-catenin-actin interaction (Figure 4B), and 4) the loss in actin bundling activity (Figure 4C) were found to be significantly stronger in Sertoli cells transfected with rpS6 mutant vs WT rpS6, illustrating that p-rpS6 played a more critical role in these events. Collectively, p-rpS6 was able to reorganize F-actin network at the BTB via its effects to redistribute and activate the Arp2/3 complex at the Sertoli cell-cell interface, resulting in cortical F-actin branching, by reorganizing actin microfilaments from a bundled to an unbundled/branched configuration, thereby impeding the TJ barrier by attenuating the structural support for TJ and basal ES proteins from the underlying actin microfilament bundles. Thus,

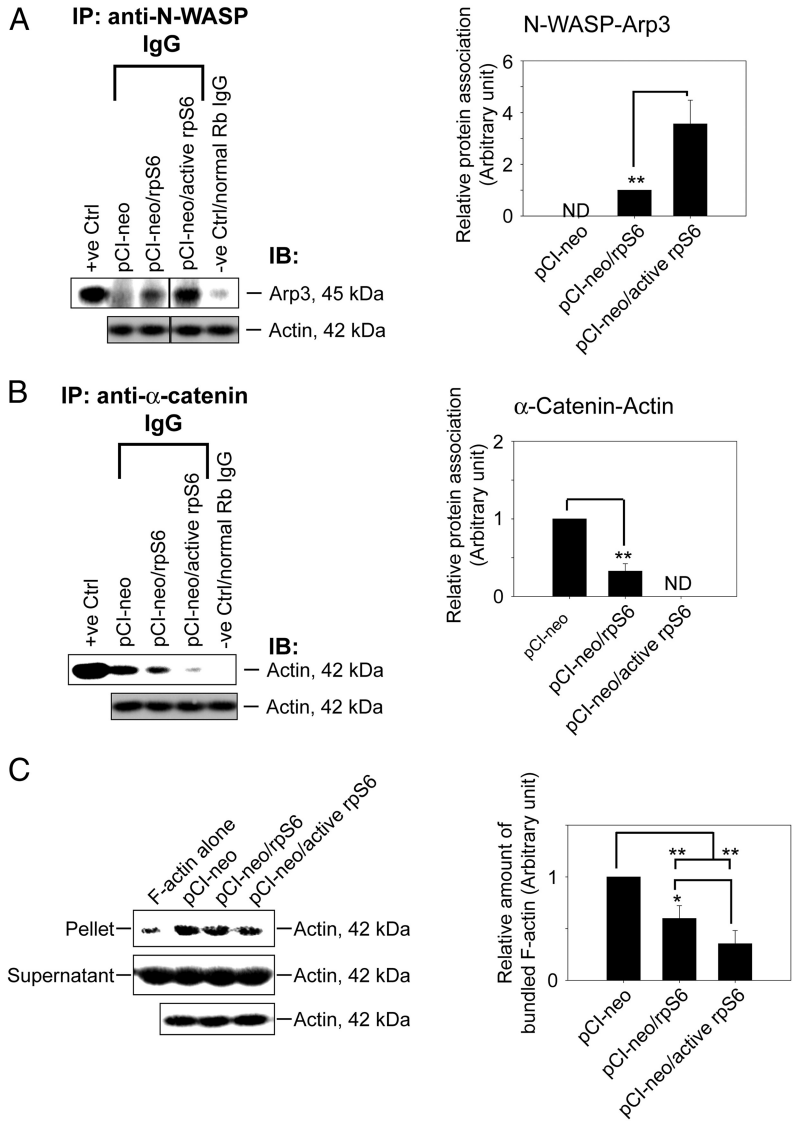

Figure 4. Overexpression of quadruple rpS6 phosphomimetic mutant in Sertoli cells shifted actin cytoskeleton from bundled to branched configuration mediated by Arp3. Sertoli cells cultured for 2 days with an established TJ barrier were transfected with corresponding vector for 18 hours. Two days after transfection, cells were harvested to obtain lysates for Co-IP and actin bundling assay. A, Co-IP that accessed protein-protein association of N-WASP and Arp3 was performed using Sertoli cell lysates (left panel). Cell lysates (~400-μg protein) incubated with normal rabbit IgG instead of precipitating antibody served as a negative control. Lysate (5-μg protein) from cells transfected with empty vector without Co-IP served as a positive control with β-actin as the protein loading control. Data are representative results of n = 4 experiments. A histogram (right panel) summarizing Co-IP results shown on the left panel. Each data point was first normalized against the corresponding actin level and then against the protein-protein interaction level in pCI-neo (control) or pCI-neo/rpS6, which was arbitrarily set at 1. Each bar is a mean ± SD of 4 independent experiments. **, $P < .01$. ND, not detectable because the level of a target protein was too low or it could not be consistently detected in multiple experiments. B, Co-IP that assessed changes in the association between α-catenin and actin using Sertoli cell lysates (left panel) under the experimental conditions as described in A. A histogram (right panel) summarizes Co-IP results from 4 experiments. ND, not detectable. **, $P < .01$. C, Lysate obtained from Sertoli cells transfected with different corresponding vector was assessed for actin bundling activity (left panel). Linear and unbundled actin filaments were found in supernatant whereas bundled F-actin were sedimented in the pellet after centrifugation (see Materials and Methods). Free F-actin without incubation with cell lysates (F-actin alone) served as a negative control, illustrating that Sertoli cell lysate was capable of bundling actin microfilaments. Data are representative findings of 4 experiments. A histogram (right panel) summarizes results shown in the left panel. Each data point was normalized against the corresponding actin level and then against the protein level in pCI-neo, which was arbitrarily set at 1. Each bar is a mean ± SD of 4 independent assays. *, $P < .05$; **, $P < .01$.

this could account for the down-regulation of TJ proteins such as occludin and claudin-11 as they were mislocalized and plausibly subjected to endocytic vesicle-mediated degradation and/or a reduced synthesis. It was expected that when the actin nucleation factor Arp2/3 complex (45) was activated in Sertoli cells following overexpression of WT rpS6 or its mutant, actin polymerization rate would have been stimulated. Surprisingly, the reverse was noted as shown in an assay that monitored the ability of cell lysate to polymerize G-actin to F-actin (Figure 5A). It is likely that after transfection of WT or active rpS6, actin polymerization promoted by the Arp2/3 complex was limited to the cell-cell interface, but the overall polymerization activity in the Sertoli cell as a whole was in fact reduced. Indeed, this possibility is supported by the F-actin staining data of Figure 3C, illustrating that an overall reduction in F-actin bundles was detected, especially in the cytosol across all the Sertoli cells after overexpression of WT or rpS6 mutant (Figure 3C). Also, the postulate that p-rpS6 induces redistribution of Arp2/3 complex to the cell-cell interface for BTB restructuring was supported by findings that at stage late VIII–IX, p-rpS6 was indeed colocalized with Arp3 at the BTB (Figure 5B), illustrating that the Arp2/3 complex was being used to induce actin reorganization to support BTB remodeling.

Knockdown of Akt1 and Akt2 by RNAi mimics the phenotype detected by overexpressing WT or rpS6 quadruple phosphomimetic mutant at the Sertoli cell BTB

Data reported in Figure 2 have shown that phosphorylations of Akt1 at Ser473 and Akt2 at Ser474 were significantly reduced after overexpression of WT rpS6 and were fur-

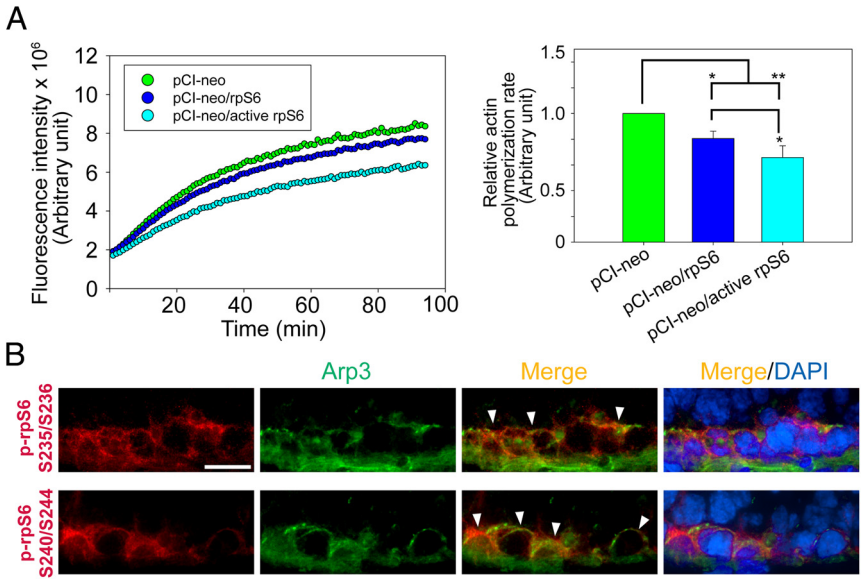

Figure 5. A study to assess effects of p-rpS6 on Sertoli cell actin polymerization kinetics at the BTB in vitro, and colocalization of p-rpS6 S235/S236 and S240/S244 with Arp3 at the BTB in vivo. A, Sertoli cells cultured for 2 days with an established TJ barrier were transfected with different vectors for 18 hours. Two days after transfection, cells were harvested to obtain lysates to assess actin polymerization kinetics. Results shown on the left panel illustrate the kinetics of actin polymerization in cells. These findings are representative data of a single experiment with n = 4 experiments that yielded similar results. Histogram shown on the right panel is the composite data, depicting the rate of actin polymerization, which was estimated by the increase in fluorescence intensity over time during the initial linear phase in the first 14 minutes of the actin polymerization assay shown on the left panel, which was estimated by linear regression in which the rate of actin polymerization in pCI-neo was arbitrarily set at 1. Each bar is a mean ± SD of n = 4 experiments. *, $P < .05$; **, $P < .01$. B, Immunofluorescence colocalization of p-rpS6-Ser235/Ser236 (red) or p-rpS6-Ser240/Ser244 (red) vs Arp3 (green) at the BTB using frozen sections of normal adult rat testes. The spatiotemporal expression of p-rpS6 coincided with the appearance of Arp3 at stage VIII of the cycle. Nuclei were stained with DAPI (blue). Scale bar, 25 μm.

ther reduced by rpS6 mutant. Note that besides promoting cell survival, p-Akt is also known to be involved in actin organization (46). We, thus, sought to examine the role of Akt in rpS6-mediated actin microfilament dynamics at the BTB by Akt knockdown using RNAi. We elected to focus on Akt 1/2 because these 2 Akt isoforms are ubiquitously found in mammalian cells whereas Akt3 is mainly expressed in brain, heart, and kidney (47). Results showed that the Sertoli cell TJ barrier was disrupted (Figure 6A) after Akt1 and Akt2 was knockdown by approximately 50% (Figure 6, B and C). In addition, after a knockdown of Akt1/2, approximately 50% drop in both p-Akt1-Ser473 and p-Akt2-Ser474 was detected (Figure 6, B and C). More important, actin microfilaments in Sertoli cells were reorganized, in which considerably less actin microfilaments bundles were present in the cytosol after Akt silencing, and many of these actin microfilaments were truncated (Figure 6D). This actin cytoskeleton remodeling was likely contributed by an up-regulation of p-FAK-Tyr^{407} (Figure 6, B and C). Also, this induction of p-FAK-Tyr^{407} probably caused a redistribution of the activated Arp2/3 complex at the cell-cell interface, which was shown by an increase in Arp3 localization at the cortical side of Sertoli cells (Figure 6D). Furthermore, this was also accompanied by a robust increase in N-WASP-Arp3 association as demonstrated by Co-IP (Figure 6, E and F). As mentioned before, this activation of Apr2/3 complex at the cortical side could perturb the TJ-permeability barrier function, because branching of actin microfilaments led to a reduction in F-actin bundles to support adhesion protein complexes of the TJ and basal ES at the BTB. This notion is supported by a significant reduction in α-catenin-actin association in Akt1/2-silenced cells (Figure 6, E and F).

Discussion

Previous studies that examined mTORC1 and its downstream molecule rpS6 were focused mostly on their role in protein synthesis (39, 48–50). A recent study, however, has demonstrated that rpS6 knockdown by RNAi leads to changes in F-actin reorganization using the Sertoli BTB as a study model (16), illustrating that the rpS6-mediated mTORC1 action has other yet-to-be identified cellular functions besides protein synthesis, consistent with recent findings that mTOR is involved in actin cytoskeleton regulation in mammalian cells and/or tissues (20, 51–53). The notion that rpS6 is involved in actin microfilament organization is confirmed unequivocally here that F-actin organization in Sertoli cells is modified by overexpression of a constitutively active rpS6 mutant. However, it is unexpected that the overall actin polymerization rate was in fact reduced in Sertoli cells overexpressed with WT or p-rpS6 mutant despite an activation of the actin nucleating factor Arp2/3 complex. Although F-actin branching activity was robustly taken place at the cell-cell interface, an overall reduction of F-actin bundles were found across the entire Sertoli cell cytosol with many truncated microfilaments. It should be cautioned to note that in addition to the Arp2/3 complex, other actin regulatory proteins are possibly involved in the p-rpS6-induced actin remodeling. For example, cofilin, which

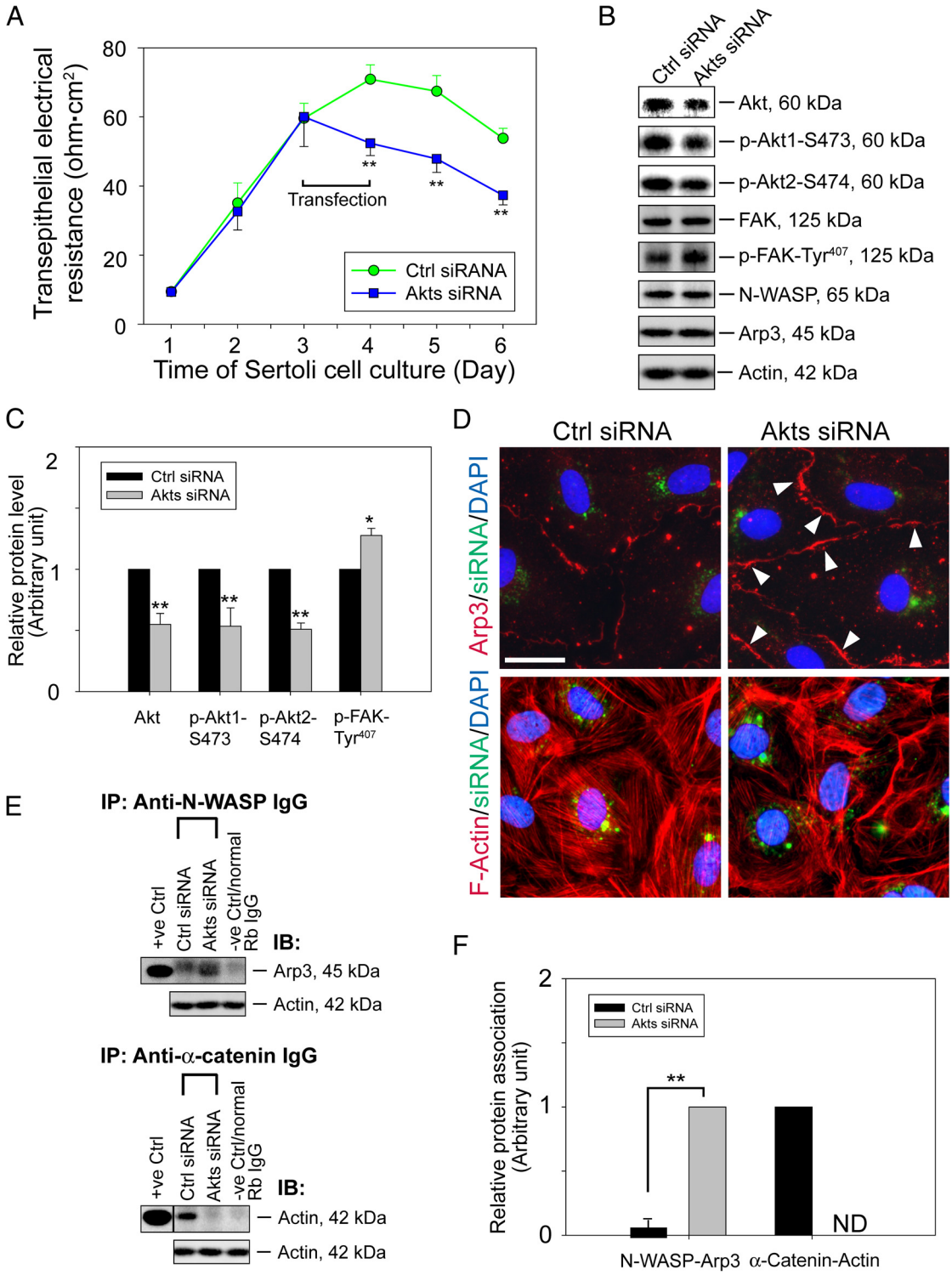

Figure 6. rpS6-induced F-actin reorganization at the Sertoli cell BTB through Akt signaling. A, On day 3, Sertoli cells were transfected with Akt1 and Akt2 siRNA duplexes for 24 hours. Thereafter, changes in the TJ barrier were assessed. Each data point is a mean ± SD of 4 replicates of an experiment, and n = 3 experiments yielded similar results. **, $P < .01$ vs corresponding controls. B, Effects of Akt1/2 knockdown that silenced Akt, p-Akt-S473, and p-Akt-S474 expression by approximately 50% on the expression of selected actin regulatory proteins on day 5 of culture with β-actin served as the loading control. Data are representative findings of 4 experiments. C, Histograms summarizing immunoblotting data of B. Proteins that did not show any significant changes were not shown. Each data point was first normalized against the corresponding actin level and then against the protein level in Ctrl siRNA, which was arbitrarily set at 1. Each bar is a mean ± SD of 4 experiments. *, $P < .05$; **, $P < .01$. D, Changes in the localization of Arp3 (red) or the organization of F-actin (red) in Sertoli cells on day 5 were examined after cells were transfected on day 3 (for 24 h) with siRNA duplexes and cotransfected with siGLO (green fluorescence) to assess transfection efficacy. Nuclei were stained with DAPI (blue). Akt1/2 knockdown caused Arp3 to relocalize to the cell-cell interface from cell cytosol (annotated by white arrowheads), inducing

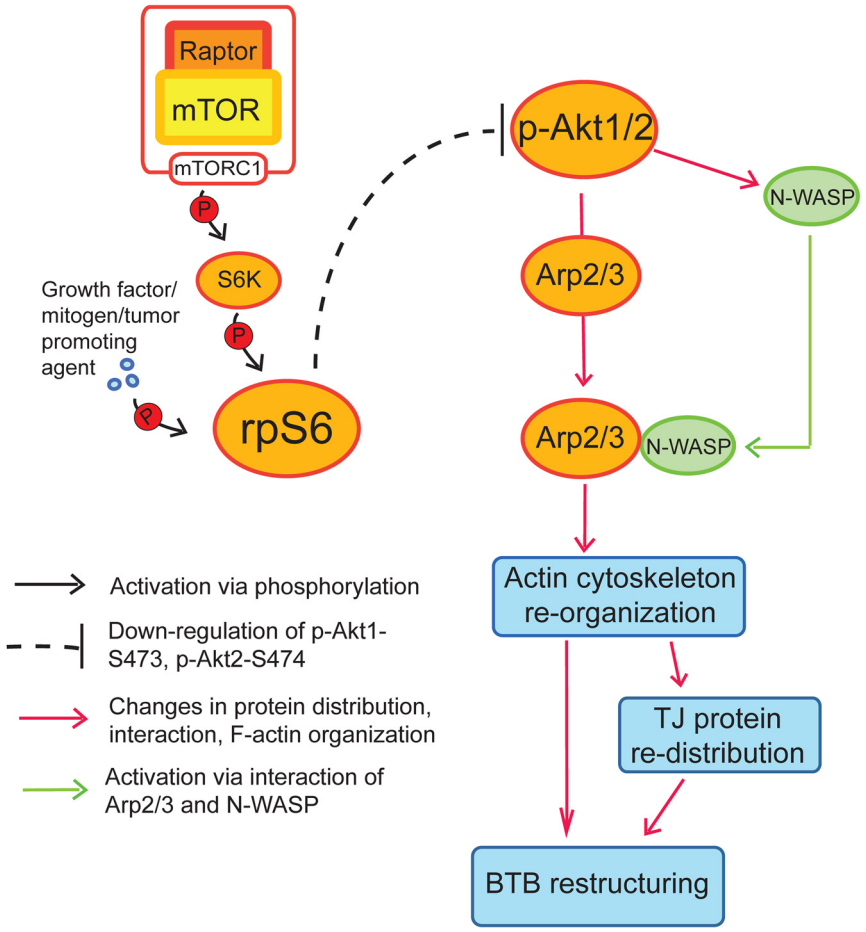

Figure 7. A schematic drawing that illustrates the cascade of events in mTORC1-mediated F-actin reorganization at the BTB via rpS6 downstream. rpS6 activated via phosphorylation by mTORC1 and S6K (ribosomal S6 kinase, such as p70 S6K) down-regulates the expression of p-Akt1-S473 and p-AKt2-S474, which in turn activates the Arp2/3 complex via an increase in N-WASP-Arp2/3 association, as well as changes in the localization of the Arp2/3 complex in the Sertoli cell epithelium. This, thus, induces changes in the organization of actin microfilaments at the BTB, causing BTB remodeling. This hypothesis is supported by findings in this report.

promotes actin depolymerization by severing actin filaments (54), can likely be activated to maintain the pool of G-actin for actin nucleation triggered by the Arp2/3 complex after its activation by N-WASP (55), resulting from overexpression of the quadruple phosphomimetic rpS6 mutant. Thus, although the Arp2/3 complex is activated to promote nucleation of F-actin at the cortical side, the combined effects of all the actin regulatory proteins in the entire Sertoli cell epithelium after overexpression of WT or p-rpS6 mutant can contribute to a reduced rate of actin polymerization.

The underlying mechanism by which p-rpS6 exerts its effects on F-actin organization appears to be unrelated to changes in protein synthesis such as by modulating the pool of actin regulatory proteins (eg, Arp3, N-WASP, Eps8) at the Sertoli cell BTB, because the steady-state level of these proteins remained relatively unaltered after overexpression of WT rpS6 or its mutant based on immunoblot analysis. However, the involvement of p-rpS6 in mediating changes in protein synthesis cannot be completely ruled out, because p-rpS6 could still alter de novo synthesis of other actin regulatory proteins that were not examined in our study. On the other hand, overexpression of p-rpS6 mutant was found to perturb the localization of TJ integral membrane proteins at the Sertoli cell-cell interface, such as occludin and claudin-11, whereby these proteins were found to be redistributed, moved away from the cell-cell interface. Perhaps these integral membrane proteins were internalized via an induction of endocytosis, to be followed by endosome-mediated degradation, because the steady-state protein level of occludin and claudin-11 was shown to be significantly reduced in Sertoli cells after overexpression of rpS6 mutant. In short, these changes in the localization of occludin and claudin-11 at the cell-cell interface and a considerably down-regulation of their expression are likely the result of an alteration in endocytic vesicle-mediated trafficking events. These changes are only possible due to reorganization of the underlying F-actin network at or near the cell surface in the epithelial cells (56–58). Alternatively, this can be the result of a reduced synthesis of these proteins after overexpression of rpS6 mutant in Sertoli cells, because rpS6 is a known regulator of protein synthesis (39, 48–50). Taking collectively, these findings are in agreement with the basic function of rpS6 and mTORC1, in which this signaling pathway exerts its effects via changes in protein synthesis of its target proteins, such as occludin, claudin-11, p-FAK-Tyr^{407}, and other actin regulatory proteins, includ-

Figure 6. (Continued). F-actin reorganization, in which truncated microfilaments was found near the cell surface; and microfilaments no longer well organized in cytosol and cell cortex. Scale bar, 50 μm. E, Sertoli cell lysates (~400-μg protein) obtained on day 5 were subjected to Co-IP to assess changes in association between N-WASP and Arp3 or between α-catenin and actin. Cell lysate incubated with normal rabbit IgG served as a negative control; cell lysate (5-μg protein) from cells transfected with control duplexes without Co-IP served as a positive control with β-actin as the protein loading control. Data are representative findings of 4 experiments. F, Histograms summarizing results shown in E. ND, not detectable, illustrating that the extent of protein-protein association could not be consistently detected. Each bar is a mean ± SD of 4 experiments. **, $P < .01$.

ing nonreceptor protein tyrosine kinases (eg, c-Yes, c-Src), which are known to perturb actin microfilament organization at the BTB and involved in endocytic vesicle-mediated trafficking (15, 59).

Here, we also demonstrated that the p-rpS6-induced disruptive effects on F-actin organization at the Sertoli cell BTB is mediated through Akt, which is a Ser/Thr protein kinase known to play a key role in glucose metabolism, apoptosis, proliferation, transcription, cell migration, and tissue barrier function (60–62). This conclusion was reached based on findings here in which a knockdown of Akt1/2 by RNAi mimics the phenotype detected by overexpressing phosphomimetic rpS6 mutant in Sertoli cells, such as a disruption of actin microfilaments in Sertoli cells, including truncation and misorganization, as well as an up-regulation of p-FAK-Tyr^{407}. Furthermore, studies using specific inhibitors also support the notion that Akt is a regulator that modulates rpS6-mediated Sertoli cell BTB function (21). Additionally, Akt is also a downstream regulator of mTORC2 signaling complex (39, 62). Taken together, these findings, thus, suggest that Akt/protein kinase B may serve as the effector molecule of mTORC1 and mTORC2 in the testis in response to the stage of the epithelial cycle during spermatogenesis. Also, phosphorylation of rpS6 is known to be stimulated by growth factors, mitogens and other tumor-inducing agents (63–65); thus, other molecules besides Akt may also contribute to the overall regulation of this pathway. In brief, mTORC1 was shown to promote BTB disruption (16), whereas mTORC2 promotes BTB integrity (17), and these 2 signaling complexes are having antagonistic effects on the Sertoli cell TJ-barrier function. Thus, the concerted efforts of mTORC1 and mTORC2 provide a novel mechanism to "close" and "open" the TJ barrier to facilitate the transport of preleptotene spermatocytes at the BTB microenvironment, such as at stage VIII of the epithelial cycle, which is likely mediated by changes in the organization of actin microfilaments besides an alteration of protein synthesis. In this context, it is of interest to note that because several findings based on the use of this in vitro Sertoli cell system to study BTB function have been validated in studies in vivo (32, 34–37), data reported here are, thus, relevant to the Sertoli cell BTB function in vivo. It is obvious that future studies should include an analysis of the testis in vivo.

In summary, rpS6 regulates Sertoli cell BTB through Akt1/2, which in turn modulates the organization of F-actin, regulating adhesion function at the cell-cell interface (Figure 7), providing an efficient mechanism to facilitate preleptotene spermatocyte transport across the BTB in stage VIII tubules.

Acknowledgments

Address all correspondence and requests for reprints to: C. Yan Cheng, PhD, The Mary M. Wohlford Laboratory for Male Contraceptive Research, Center for Biomedical Research, Population Council, 1230 York Avenue, New York, NY 10065. E-mail: y-cheng@popcbr.rockefeller.edu.

This work was supported by grants from the National Institutes of Health, the *Eunice Kennedy Shriver* National Institute of Child Health and Human Development (NICHD) R01 HD0560334 (to C.Y.C.) and U54 HD029990 Project 5 (to C.Y.C.); the Hong Kong Research Grants Council (RGC) General Research Fund 771513 (to W.M.L.), the National Science Foundation of China/RGC Joint Research Scheme N_HKU717/12 (to W.M.L.), and the Committee on Research and Conference Grants (University of Hong Kong) seed funding (to W.M.L.).

Disclosure Summary: The authors have nothing to disclose.

References

1. **Schlatt S, Ehmcke J.** Regulation of spermatogenesis: an evolutionary biologist's perspective. *Semin Cell Dev Biol*. 2014;29:2–16.
2. **O'Shaughnessy PJ.** Hormonal control of germ cell development and spermatogenesis. *Semin Cell Dev Biol*. 2014;29:55–65.
3. **de Mateo S, Sassone-Corsi P.** Regulation of spermatogenesis by small non-coding RNAs: role of the germ granule. *Semin Cell Dev Biol*. 2014;29:84–92.
4. **Cheng CY, Mruk DD.** The blood-testis barrier and its implications in male contraception. *Pharmacol Rev*. 2012;64:16–64.
5. **França LR, Auharek SA, Hess RA, Dufour JM, Hinton BT.** Blood-tissue barriers: morphofunctional and immunological aspects of the blood-testis and blood-epididymal barriers. *Adv Exp Med Biol*. 2012;763:237–259.
6. **Pelletier RM.** The blood-testis barrier: the junctional permeability, the proteins and the lipids. *Prog Histochem Cytochem*. 2011;46:49–127.
7. **Russell L.** Movement of spermatocytes from the basal to the adluminal compartment of the rat testis. *Am J Anat*. 1977;148:313–328.
8. **Russell L.** Observations on rat Sertoli ectoplasmic ('junctional') specializations in their association with germ cells of the rat testis. *Tissue Cell*. 1977;9:475–498.
9. **Russell LD.** The blood-testis barrier and its formation relative to spermatocyte maturation in the adult rat: a lanthanum tracer study. *Anat Rec*. 1978;190:99–111.
10. **Yan HH, Mruk DD, Lee WM, Cheng CY.** Blood-testis barrier dynamics are regulated by testosterone and cytokines via their differential effects on the kinetics of protein endocytosis and recycling in Sertoli cells. *FASEB J*. 2008;22:1945–1959.
11. **Smith BE, Braun RE.** Germ cell migration across Sertoli cell tight junctions. *Science*. 2012;338:798–802.
12. **Cheng CY, Mruk DD.** A local autocrine axis in the testes that regulates spermatogenesis. *Nature Rev Endocrinol*. 2010;6:380–395.
13. **Wang RS, Yeh S, Tzeng CR, Chang C.** Androgen receptor roles in spermatogenesis and fertility: lessons from testicular cell-specific androgen receptor knockout mice. *Endocr Rev*. 2009;30:119–132.
14. **Su L, Mruk DD, Lee WM, Cheng CY.** Differential effects of testosterone and TGF-β3 on endocytic vesicle-mediated protein trafficking events at the blood-testis barrier. *Exp Cell Res*. 2010;316:2945–2960.
15. **Xiao X, Mruk DD, Wong EW, et al.** Differential effects of c-Src and c-Yes on the endocytic vesicle-mediated trafficking events at the Sertoli cell blood-testis barrier: an in vitro study. *Am J Physiol Endocrinol Metab*. 2014;307:E553–E562.

16. **Mok KW, Mruk DD, Silvestrini B, Cheng CY.** rpS6 regulates blood-testis barrier dynamics by affecting F-actin organization and protein recruitment. *Endocrinology*. 2012;153:5036–5048.
17. **Mok KW, Mruk DD, Lee WM, Cheng CY.** Rictor/mTORC2 regulates blood-testis barrier dynamics via its effects on gap junction communications and actin filament network. *FASEB J*. 2013;27:1137–1152.
18. **Vogl AW, Vaid KS, Guttman JA.** The Sertoli cell cytoskeleton. *Adv Exp Med Biol*. 2008;636:186–211.
19. **Huang K, Fingar DC.** Growing knowledge of the mTOR signaling network. *Sem Cell Dev Biol*. 2014;36C:79–90.
20. **He Y, Li D, Cook SL, et al.** Mammalian target of rapamycin and Rictor control neutrophil chemotaxis by regulating Rac/Cdc42 activity and the actin cytoskeleton. *Mol Biol Cell*. 2013;24:3369–3380.
21. **Mok KW, Mruk DD, Cheng CY.** rpS6 regulates blood-testis barrier dynamics through Akt-mediated effects on MMP-9. *J Cell Sci*. 2014;127:4870–4882.
22. **Lie PP, Mruk DD, Mok KW, Su L, Lee WM, Cheng CY.** Focal adhesion kinase-Tyr^{407} and -Tyr^{397} exhibit antagonistic effects on blood-testis barrier dynamics in the rat. *Proc Natl Acad Sci USA*. 2012;109:12562–12567.
23. **Mruk DD, Cheng CY.** An *in vitro* system to study Sertoli cell blood-testis barrier dynamics. *Methods Mol Biol*. 2011;763:237–252.
24. **Li MW, Mruk DD, Lee WM, Cheng CY.** Connexin 43 and plakophilin-2 as a protein complex that regulates blood-testis barrier dynamics. *Proc Natl Acad Sci USA*. 2009;106:10213–10218.
25. **Siu MK, Wong CH, Lee WM, Cheng CY.** Sertoli-germ cell anchoring junction dynamics in the testis are regulated by an interplay of lipid and protein kinases. *J Biol Chem*. 2005;280:25029–25047.
26. **Lee NP, Cheng CY.** Regulation of Sertoli cell tight junction dynamics in the rat testis via the nitric oxide synthase/soluble guanylate cyclase/3′,5′-cyclic guanosine monophosphate/protein kinase G signaling pathway: an *in vitro* study. *Endocrinology*. 2003;144:3114–3129.
27. **Li MW, Mruk DD, Lee WM, Cheng CY.** Disruption of the blood-testis barrier integrity by bisphenol A in vitro: is this a suitable model for studying blood-testis barrier dynamics? *Int J Biochem Cell Biol*. 2009;41:2302–2314.
28. **Janecki A, Jakubowiak A, Steinberger A.** Effect of cadmium chloride on transepithelial electrical resistance of Sertoli cell monolayers in two-compartment cultures–a new model for toxicological investigations of the "blood-testis" barrier *in vitro*. *Toxicol Appl Pharmacol*. 1992;112:51–57.
29. **Kaitu'u-Lino TJ, Sluka P, Foo CF, Stanton PG.** Claudin-11 expression and localisation is regulated by androgens in rat Sertoli cells *in vitro*. *Reproduction*. 2007;133:1169–1179.
30. **Okanlawon A, Dym M.** Effect of chloroquine on the formation of tight junctions in cultured immature rat Sertoli cells. *J Androl*. 1996;17:249–255.
31. **Chen J, Fok KL, Chen H, Zhang XH, Xu WM, Chan HC.** Cryptorchidism-induced CFTR down-regulation results in disruption of testicular tight junctions through up-regulation of NF-κB/COX-2/PGE_2. *Hum Reprod*. 2012;27:2585–2597.
32. **Qiu L, Zhang X, Zhang X, et al.** Sertoli cell is a potential target for perfluorooctane sulfonate-induced reproductive dysfunction in male mice. *Toxicol Sci*. 2013;135:229–240.
33. **Du M, Young J, De Asis M, et al.** A novel subcellular machine contributes to basal junction remodeling in the seminiferous epithelium. *Biol Reprod*. 2013;88:60.
34. **Lui WY, Wong CH, Mruk DD, Cheng CY.** TGF-β3 regulates the blood-testis barrier dynamics via the p38 mitogen activated protein (MAP) kinase pathway: an *in vivo* study. *Endocrinology*. 2003;144:1139–1142.
35. **Su L, Mruk DD, Lie PPY, Silvestrini B, Cheng CY.** A peptide derived from laminin-γ3 reversibly impairs spermatogenesis in rats. *Nat Communs*. 2012;3:1185.
36. **Nicholls PK, Harrison CA, Gilchrist RB, Farnworth PG, Stanton PG.** Growth differentiation factor 9 is a germ cell regulator of Sertoli cell function. *Endocrinology*. 2009;150:2481–2490.
37. **Wong CH, Mruk DD, Lui WY, Cheng CY.** Regulation of blood-testis barrier dynamics: an *in vivo* study. *J Cell Sci*. 2004;117:783–798.
38. **Mruk DD, Cheng CY.** Enhanced chemiluminescence (ECL) for routine immunoblotting: an inexpensive alternative to commercially available kits. *Spermatogenesis*. 2011;1:121–122.
39. **Mok KW, Mruk DD, Cheng CY.** Regulation of blood-testis barrier (BTB) dynamics during spermatogenesis via the "Yin" and "Yang" effects of mammalian target of rapamycin complex 1 (mTORC1) and mTORC2. *Int Rev Cell Mol Biol*. 2013;301:291–358.
40. **Inoki K, Li Y, Zhu T, Wu J, Guan KL.** TSC2 is phosphorylated and inhibited by AKT and suppresses mTOR signalling. *Nat Cell Biol*. 2002;4:648–657.
41. **Ruvinsky I, Meyuhas O.** Ribosomal protein S6 phosphorylation: from protein synthesis to cell size. *Trends Biochem Sci*. 2006;31:342–348.
42. **Serrels B, Serrels A, Brunton VG, et al.** Focal adhesion kinase controls actin assembly via a FERM-mediated interaction with the Arp2/3 complex. *Nat Cell BIol*. 2007;9:1046–1056.
43. **Yonemura S.** Cadherin-actin interactions at adherens junctions. *Curr Opin Cell Biol*. 2011;23:515–522.
44. **Harris TJ, Tepass U.** Adherens junctions: from molecules to morphogenesis. *Nat Rev Mol Cell Biol*. 2010;11:502–514.
45. **Vartiainen MK, Machesky LM.** The WASP-Arp2/3 pathway: genetic insights. *Curr Opin Cell Biol*. 2004;16:174–181.
46. **Chin YR, Toker A.** Akt isoform-specific signaling in breast cancer: uncovering an anti-migratory role for palladin. *Cell Adh Migr*. 2011;5:211–214.
47. **Masure S, Haefner B, Wesselink JJ, et al.** Molecular cloning, expression and characterization of the human serine/threonine kinase Akt-3. *Eur J Biochem*. 1999;265:353–360.
48. **Magnuson B, Ekim B, Fingar DC.** Regulation and function of ribosomal protein S6 kinase (S6K) within mTOR signalling networks. *Biochem J*. 2012;441:1–21.
49. **Meyuhas O, Dreazen A.** Ribosomal protein S6 kinase from TOP mRNAs to cell size. *Prog Mol Biol Transl Sci*. 2009;90:109–153.
50. **Morita M, Gravel SP, Hulea L, et al.** mTOR coordinates protein synthesis, mitochondrial activity and proliferation. *Cell Cycle*. 2015;14:473–480.
51. **Angliker N, Rüegg MA.** In vivo evidence for mTORC2-mediated actin cytoskeleton rearrangement in neurons. *Bioarchitecture*. 2013;3:113–118.
52. **Chen MB, Wei MX, Han JY, et al.** MicroRNA-451 regulates AMPK/mTORC1 signaling and fascin1 expression in HT-29 colorectal cancer. *Cell Signal*. 2014;26:102–109.
53. **Imam JS, Plyler JR, Bansal H, et al.** Genomic loss of tumor suppressor miRNA-204 promotes cancer cell migration and invasion by activating AKT/mTOR/Rac1 signaling and actin reorganization. *PLoS One*. 2012;7:e52397.
54. **Hild G, Kalmár L, Kardos R, Nyitrai M, Bugyi B.** The other side of the coin: functional and structural versatility of ADF/cofilins. *Eur J Cell Biol*. 2014;93:238–251.
55. **Chiu TT, Patel N, Shaw AE, Bamburg JR, Klip A.** Arp2/3- and cofilin-coordinated actin dynamics is required for insulin-mediated GLUT4 translocation to the surface of muscle cells. *Mol Biol Cell*. 2010;21:3529–3539.
56. **Rougerie P, Miskolci V, Cox D.** Generation of membrane structures during phagocytosis and chemotaxis of macrophages: role and regulation of the actin cytoskeleton. *Immunol Rev*. 2013;256:222–239.
57. **Loebrich S.** The role of F-actin in modulating clathrin-mediated endocytosis: lessions from neurons in health and neuropsychiatric disorder. *Commun Integr Biol*. 2014;7:e28740.
58. **Mooren OL, Galletta BJ, Cooper JA.** Roles for actin assembly in endocytosis. *Annu Rev Biochem*. 2012;81:661–686.
59. **Xiao X, Mruk DD, Cheng CY.** c-Yes regulates cell adhesion at the

apical ectoplasmic specialization-blood-testis barrier axis via its effects on protein recruitment and distribution. *Am J Physiol Endocrinol Metab*. 2013;304:E145–E159.
60. **Shisheva A.** PtdIns5P: news and views of its appearance, disappearance and deeds. *Arch Biochem Biophys*. 2013;538:171–180.
61. **Stambolic V, Woodgett JR.** Functional distinctions of protein kinase B/Akt isofroms defined by their influence on cell migration. *Tends Cell Biol*. 2006;16:461–466.
62. **Fayard E, Xue G, Parcellier A, Bozulic L, Hemmings BA.** Protein kinase B (PKB/Akt), a key mediator of the PI3K signaling pathway. *Curr Top Microbiol Immunol*. 2010;346:31–56.
63. **Kang MH, Kim IH, Nam TJ.** Phloroglucinol induces apoptosis through the regulation of insulin-like growth factor 1 receptor signaling pathways in human colon cancer HT-29 cells. *Int J Oncol*. 2014;45:1036–1042.
64. **Jansson N, Rosario FJ, Gaccioli F, et al.** Activation of placental mTOR signaling and amino acid transporters in obese women giving birth to large babies. *J Clin Endocrinol Metab*. 2013;98:105–113.
65. **Papageorgiou A, Avruch J.** A genome-wide RNAi screen for polypeptides that alter rpS6 phosphorylation. *Methods Mol Biol*. 2012; 821:187–214.